Article

Comparative Study of Magnetic Properties of (Mn$_{1-x}$A$_x^{IV}$)Bi2Te4 A$_x^{IV}$ = Ge, Pb, Sn

Dmitry A. Estyunin *, Anna A. Rybkina, Konstantin A. Kokh, Oleg E. Tereshchenko, Marina V. Likholetova, Alexander M. Shikin

Posted Date: 25 July 2023

doi: 10.20944/preprints202307.1640.v1

Keywords: Topological insulators; Modification of magnetic properties; Antiferromagnetics; Doping; SQUID magnetometry; ARPES

Article

Comparative Study of Magnetic Properties of $(Mn_{1-x}A^{IV}_x)Bi_2Te_4$ A^{IV} = Ge, Pb, Sn

Dmitry A. Estyunin [1,*], Anna A. Rybkina [1], Konstantin A. Kokh [1,2], Oleg E. Tereshchenko [1,3,4], Marina V. Likholetova [1] and Alexander M. Shikin [1]

1 Department of Physics, Saint Petersburg State University, 198504 St. Petersburg, Russia
2 Sobolev Institute of Geology and Mineralogy, Siberian Branch, Russian Academy of Sciences, 630090 Novosibirsk, Russia
3 Rzhanov Institute of Semiconductor Physics, Siberian Branch, Russian Academy of Sciences, 630090 Novosibirsk, Russia
4 Synchrotron Radiation Facility SKIF, Boreskov Institute of Catalysis, Siberian Branch, Russian Academy of Sciences, 630559 Kol'tsovo, Russia
* Correspondence: estyunin@gmail.com

Abstract: We investigated the magnetic properties of antiferromagnetic (AFM) topological insulator $MnBi_2Te_4$ with partial substitution of Mn atoms by non-magnetic elements (A^{IV} = Ge, Pb, Sn). Samples with various element concentrations (10-80%) were studied using SQUID magnetometry. The results demonstrate that, for all substitutes the type of magnetic ordering remains AFM, while the Nèel temperature (T_N) and spin-flop transition field (H_{SF}) decrease with increasing A^{IV} = Ge, Pb, Sn concentration. The rate of decrease varies among the elements, being highest for Pb, followed by Sn and Ge. This behavior is attributed to combined effects of magnetic dilution and lattice parameter increase on magnetic properties, most prominent in $(Mn_{1-x}Pb_x)Bi_2Te_4$. Besides this, the linear approximation of experimental data of T_N and H_{SF} suggests higher magnetic parameters for pure $MnBi_2Te_4$ than observed experimentally, indicating the possibility of their non-monotonic variation at low concentrations and the potential for enhancing magnetic properties through doping $MnBi_2Te_4$ with small amounts of nonmagnetic impurities. Notably, the $(Mn_{1-x}Pb_x)Bi_2Te_4$ sample with 10% Pb substitution indeed exhibits increased magnetic parameters, which is also validated by local analyses using ARPES. Our findings shed light on tailoring the magnetic behavior of $MnBi_2Te_4$-based materials, offering insights for potential applications in device technologies.

Keywords: topological insulators; modification of magnetic properties; antiferromagnetics; doping; SQUID magnetometry; ARPES

1. Introduction

The interest in investigating magnetic topological insulators (TIs) arise primarily from their potential to manifest the quantum anomalous Hall effect (QAHE) [1–4]. In the QAHE state, edge conduction occurs in magnetic TIs, which enables the transport of spin-polarised electrons over significant distances without scattering. The remarkable aspect of magnetic TIs is that the realization of the QAHE state does not require an external magnetic field, making them highly applicable in low-power electronics and quantum computing. Among various platforms, the intrinsic antiferromagnetic (AFM) TI $MnBi_2Te_4$ has emerged as the most promising candidate for investigating the interplay between magnetism and topology, as well as achieving the QAHE state [5–9]. Recent studies have confirmed the feasibility of attaining the QAHE state in thin films of $MnBi_2Te_4$, demonstrating its transition at considerably higher temperatures compared to magnetically doped TIs [10–12].

$MnBi_2Te_4$ is a layered van der Waals crystal composed of septuple-layer (SL) blocks with each SL block arranged in a Te-Bi-Te-Mn-Te-Bi-Te configuration [13,14]. The magnetic atoms are directly incorporated into the crystal structure. This allows to significantly increase the concentration of

Preprints (www.preprints.org) | NOT PEER-REVIEWED | Posted: 25 July 2023 doi:10.20944/preprints202307.1640.v1

magnetic material in TI without disturbing the crystal structure and provides better interaction between magnetic atoms (Mn) and atoms (Bi, Te) on which topological surface states are localised. The magnetic properties of $MnBi_2Te_4$ turn out to be outstanding among other known magnetic TIs. The material exhibits A-type AFM ordering with Mn magnetic moments aligned ferromagnetically within each SL and antiferromagnetically along the c-axis between adjacent SLs. The Nèel temperature of $MnBi_2Te_4$ is approximately $24-25$ K [6,9,15–17]. The spin-flop transition field is approximately 3.5 T, and the ferromagnetic transition fields range from $7-8$ T [18].

The ability to manipulate the magnetic properties of $MnBi_2Te_4$ is an intriguing and practically significant area of research. For instance, in pure $MnBi_2Te_4$, a substantial external magnetic field of several Tesla is required to alter the current direction in the QAHE state, which ideally should be reduced. Currently, several approaches are being developed to achieve control over the magnetic properties of $MnBi_2Te_4$:

1. The first approach involves the insertion of additional (m-1) $[Bi_2Te_3]$ QLs between one $[MnBi_2Te_4]$ SL resulting in the series of compounds $MnBi_{2m}Te_{3m+1}$ with $m \geq 1$ [14,19–22]. This series includes the homologous phases $MnBi_2Te_4$ (m=1: 124), $MnBi_4Te_7$ (m=2: 147), and $MnBi_6Te_{10}$ (m=3: $16\overline{10}$), all of which can be classified as $\mathbb{Z}_2$ AFM TIs. However, as the number of $[Bi_2Te_3]$ QLs increases, significant changes occur in the magnetic properties. For the 147 phase, T_N is already 13 K and H_{SF} does not exceed 0.3 T. The phase $16\overline{10}$ possesses an uncertain type of magnetic ordering which can be either AFM or FM, depending on growth conditions and the presence of defects [23,24]. For phases with higher m, the system resembles non-interacting 2D ferromagnets formed by the $[MnBi_2Te_4]$ SL [21].
2. The second approach is to substitute Bi atoms with Sb atoms, resulting in $Mn(Bi_{1-y}Sb_y)_2Te_4$ compounds [25]. This substitution generally leads to an increase in the number of anti-site defects, such as $Mn_{Bi,Sb}$ (Mn occupying the position of Bi or Sb atoms) [26,27]. Consequently, this substitution affects the magnetic order of the SL, transforming it from ferromagnetic to ferrimagnetic [18]. By adjusting the growth parameters, it is possible to further increase the number of anti-site defects and induce a transition from antiferromagnetic to ferromagnetic behavior in the ground state [27].
3. Another way is to dilute Mn atoms with non-magnetic atoms. The A^{IV} = Ge, Pb, Sn elements can be chosen as suitable substituents. There are ternary TI compounds, such as $A^{IV}Bi_2Te_4$, with the same $R\bar{3}m$ symmetry group as $MnBi_2Te_4$ [13,28], allowing for arbitrary ratios of Mn substitution. Several studies [29–33] have demonstrated the synthesis of these crystals and confirmed the absence of additional substitution defects, as in the case of s substitution of Sb for Bi atoms.

The latter approach offers several intriguing advantages. For instance, in manganese tellurides (TeMn), the partial substitution of Mn atoms with nonmagnetic atoms (such as Ge) has been shown to increase the critical temperature of magnetic ordering [34,35]. Furthermore, introducing an additional element into the central layer can reduce structural strains in the crystal lattice. This effect is exemplified by the compound $BiSbTeSe_2$, in which the combination of four elements results in an enhanced surface conductivity [36,37]. This suggests that it may be possible to produce higher-quality crystals of $MnBi_2Te_4$-based magnetic TI through the partial substitution of Mn atoms with nonmagnetic elements. In general, such approach may have promise for further study and exploration.

In this study, we investigated the magnetic properties of $(Mn_{1-x}A^{IV}_x)Bi_2Te_4$ compounds with substitution of Mn atoms by A^{IV} = Ge, Pb, Sn atoms. Hereafter, the concentration x refers to the molar ratio of $A^{IV}/(A^{IV}+Mn)$. Crystals with nominal concentrations x equal to 10%, 20%, 50%, 60%, and 80% were synthesized. Using SQUID magnetometry, we analyzed various magnetic properties including the type and temperature of magnetic ordering, magnetic saturation and spin-flop transition fields for all samples. Additionally, for the $(Mn_{1-x}Pb_x)Bi_2Te_4$ sample with a nominal Pb concentration of 10%, which exhibited increased critical parameters, we conducted ARPES studies. These studies allow us to estimate the local magnetic ordering temperature by analyzing the temperature-dependent changes in the electronic structure, following the approach described in [17].

Preprints (www.preprints.org) | NOT PEER-REVIEWED | Posted: 25 July 2023 doi:10.20944/preprints202307.1640.v1

2. Materials and Methods

The bulk crystals of doped $MnBi_2Te_4$ (i.e. $(Mn_{1-x}A^{IV}_x)Bi_2Te_4$ where A^{IV} = Ge, Pb, Sn) were prepared by a modified Bridgman method [38,39]. The elementary Mn, Bi, Te, Ge, Pb, Sn of 4N purity were loaded into conically shaped quartz ampoules and sealed under vacuum 10^{-2} torr. The charge was synthesized by heating the ampoule to 1050 °C directly in the growth furnace. The compositions were taken according to proportions $(Mn_{1-x}A^{IV}_x)Bi_2Te_4+2\times Bi_2Te_3$. After a day of homogenization the ampoule was transferred to the cold zone (600 °C) with a speed 10 mm/day.

Thin films obtained from the ingot were initially characterized by XPS (X-ray tube with Al cathode, $h\nu = 1486$ eV). It is important to note that the characterization was performed only for the film surface, as oriented crystals were required for SQUID magnetometry measurements. The total molar fraction of Mn and A^{IV} = Ge, Pb, Sn exceeded 10%, indicating the prevalence of the 124 phase. Magnetic properties (i.e. the temperature dependences of the magnetic susceptibility $\chi(T)$ and magnetization as a function of applied magnetic field M(H) at various temperatures) were assessed using a Quantum Design MPMS 3 SQUID VSM instrument. The measurements were conducted at temperatures as low as 1.8 K, with an external magnetic field range of ± 7 T and a sensitivity of 1×10^{-8} emu at 0 T. The samples were oriented such that the external magnetic field was applied perpendicular to the crystal surface (0001), aligning with the crystallographic axis c.

ARPES measurements of a single crystal of $(Mn_{1-x}Pb_x)Bi_2Te_4$ (Pb 10% nominally) were performed at the Laser ARPES facility of the HiSOR synchrotron centre [40]. A clean surface was prepared by tape-cleavage inside a vacuum chamber with a pressure below 10^{-9} torr. The measurements were performed using a photon energy of $h\nu = 6.3$ eV with liquid helium cooling. The base pressure during the measurements remained below 5×10^{-11} torr. To obtain the dispersion dependencies at a certain temperature (temperature dependence), the sample was heated by means of an integrated heating element in the manipulator with keeping the sample position unchanged.

3. Results and Discussion

Figure 1 depicts the investigation of magnetic properties in $(Mn_{1-x}Pb_x)Bi_2Te_4$ samples, specifically the magnetic susceptibility as a function of temperature, $\chi(T)$, and the magnetization as a function of applied magnetic field, M(H). The nominal and actual concentrations of Pb are indicated at the top of the figure. The actual concentrations were determined by XPS method for the cleaved (0001) surface of the single-crystal. It is important to note that the crystal may exhibit volume inhomogeneity with regions containing excess/deficient elements or regions with different phases of the homologous series $(Mn_{1-x}A^{IV}_x)Bi_{2m}Te_{3m+1}$. The SQUID method, being sensitive to bulk properties, can reveal additional features in the measurements, such as multiple critical temperatures, multiple spin-flop transitions, or ferromagnetic hysteresis loops. It is expected that the different phases of the $(Mn_{1-x}A^{IV}_x)Bi_{2m}Te_{3m+1}$ series do not influence each other within the crystal volume, and their magnetization signals are superimposed. The samples investigated in this study exhibited various combinations of magnetization signals arising from different phases. In each sample the highest observed magnetic transition temperature and the maximum spin-flop transition field were attributed to the 124 phase. When the M(H) or $\chi(T)$ signals were relatively weak in the examined region, their derivatives ($dM(H)/dH$ and $d\chi(T)/dT$) were analyzed to identify distinctive features in the dependencies.

Preprints (www.preprints.org) | NOT PEER-REVIEWED | Posted: 25 July 2023 doi:10.20944/preprints202307.1640.v1

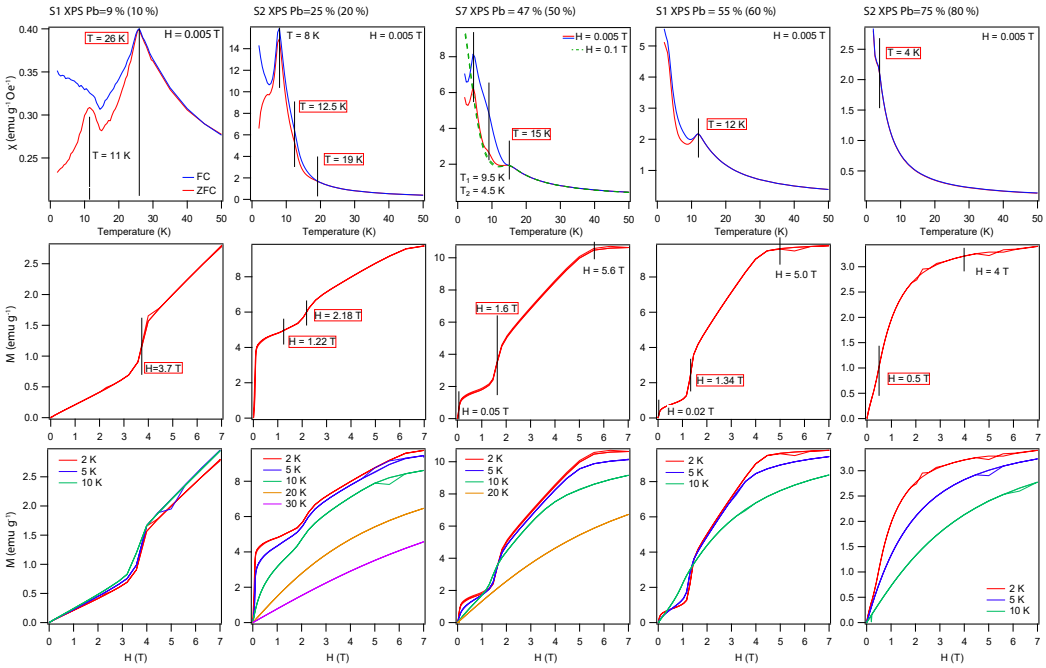

Figure 1. The temperature dependences of the magnetic susceptibility $\chi(T)$ [top line] and magnetization as a function of applied magnetic field M(H) [middle and bottom lines] were measured for $(Mn_{1-x}Pb_x)Bi_2Te_4$ samples using the SQUID method. The $\chi(T)$ measurement involved applying an external field of 5 mT (0.1 T) perpendicular to the sample surface plane along the crystallographic axis c. The red curve represents ZFC condition, while the blue curve corresponds to FC condition. The M(H) dependencies were measured at a temperature of 2 K are presented in the middle line; the M(H) curves at different temperatures are displayed on the bottom line. Critical temperature and external magnetic field values at which phase transitions occur are indicated on the panels, with the corresponding parameters for the 124 phase marked in red.

The sample with a nominal Pb concentration of 10% exhibits a $\chi(T)$ dependence that reveals the Nèel temperature of 26 K. Below this temperature, a divergence is observed between the magnetic susceptibility curves measured in ZFC conditions (red curve) and FC conditions (blue curve). This divergence arises from the presence of individual [$MnBi_2Te_4$] SL inside the crystal. The magnetic moments of these SLs can exhibit a disordered orientation along the crystallographic axis c, which corresponds to the easy magnetization axis [21]. Another AFM transition is observed at a temperature of approximately 11 K, which likely corresponds to the phase $16\overline{1}0$. Analysis of the magnetization dependence M(H) revealed that the maximum (i.e. corresponding to the 124 phase) spin-flop transition field for this sample is determined to be 3.7 T. In the low-field region another transition is detected at approximately 0.15 T (can be seen when zooming in), which rather corresponds to the $16\overline{1}0$ phase and is consistent with the results obtained from the $\chi(T)$ data.

At higher concentrations of Pb (20% nominally), the Nèel temperature of phase 124 decreases. In the investigated sample, other phases were present within the volume, and their signals dominated the measurements. However, by analyzing the derivative $d\chi(T)/dT$, it was possible to determine the Nèel temperature associated with phase 124 which is approximately 19 K. Additional AFM transition peaks were observed at temperatures of 12.5 K and 8 K. The Nèel temperature of 12.5 K is likely related to phase 147, where the Mn layer is partially diluted with Pb atoms, resulting in a slightly lower temperature compared to phase 147 without Pb atoms (13 K) [21]. However, this transition temperature may be characteristic of crystal regions with a high substitution of Mn atoms by Pb atoms (approximately $50-60\%$). Furthermore, several spin-flop transition fields were determined from the magnetization dependence M(H): 1.22 T and 2.18 T. Hence, the investigated sample likely contains two phases of 124 with different Pb concentrations.

Preprints (www.preprints.org) | NOT PEER-REVIEWED | Posted: 25 July 2023 doi:10.20944/preprints202307.1640.v1

In the sample with a Pb concentration of 47% (50% nominally), the Nèel temperature for the 124 phase is approximately 15 K. The presence of other phases is also observed in the sample. However, in measurements with a 0.1 T applied magnetic field, the signals from these phases become less pronounced, indicating that they correspond to phases 147 and higher. The spin-flop transition field for the 124 phase is determined to be 1.6 T. Additionally, magnetization saturation is observed at 5.6 T at this concentration. For the previous samples, the saturation fields were outside the measured range of $\pm$7 T. For the sample with a nominal Pb concentration of 60%, the Nèel temperature is 12 K, the spin-flop transition field is 1.34 T, and the saturation field is approximately 5 T. At a Pb concentration of 75%, the Nèel temperature decreases to 4 K, the spin-flop transition field is 0.5 T, and the saturation field is 4 T. The obtained data clearly demonstrates that the AFM type of ordering is maintained for 124 phase across all Pb concentrations up to 75%.

It is noteworthy that the AFM peak in the $\chi(T)$ dependence and the step observed in the spin-flop transition region of the M(H) dependence exhibit sharp characteristics. This suggests a homogeneous level of Mn substitution within the investigated samples. In cases where a certain range of substitution concentrations exists, one would expect a broader and more extended peak (step). Therefore, it is likely that the samples possess discrete values of substitution concentration, which can be estimated through XPS measurements conducted on the sample surface.

Further, we studied $(Mn_{1-x}A^{IV}_x)Bi_2Te_4$ samples where Mn atoms were substituted with Sn and Ge atoms (Figures 2 and 3). Overall, similar trends as observed for $(Mn_{1-x}Pb_x)Bi_2Te_4$ samples are preserved for $(Mn_{1-x}Sn_x)Bi_2Te_4$ and $(Mn_{1-x}Ge_x)Bi_2Te_4$: the critical temperature and spin-flop transition field gradually decrease, while the AFM type of magnetic ordering is maintained. However, some peculiarities may occur due to deficiencies of the investigated crystals. The samples also exhibit different phases from the homologous series $(Mn_{1-x}A^{IV}_x)Bi_{2m}Te_{3m+1}$.

No additional features were found in the $\chi(T)$ and M(H) dependencies for $(Mn_{1-x}Sn_x)Bi_2Te_4$ compared to $(Mn_{1-x}Pb_x)Bi_2Te_4$. However, when Mn is substituted with Ge in the sample with a nominal concentration of 20%, an additional feature appears in the $\chi(T)$ dependence. Unusually, a divergence between the ZFC and FC curves is observed both above and below the Nèel temperature. We attribute this to the presence of the MnTe phase in the studied sample, which also exhibits the AFM type of magnetic ordering with a critical temperature up to 300 K [41]. Interestingly, these features disappear when measurements are conducted with the application of a larger field (0.1 T). The observed spin-flop transition at a field of 3.5 T corresponds to the 124 phase. This is supported by the absence of this transition in the M(H) dependence above 30 K (see Figure 3, bottom line). Furthermore, in the $(Mn_{1-x}Ge_x)Bi_2Te_4$ sample with a nominal Ge concentration of 50%, the AFM transition peak appears relatively broad compared to other samples where the peaks are sharper. This indicates that the Ge concentration in this particular sample varies within a certain range. As a result, a range of Nèel temperatures from 16 to 19 K is observed for this sample.

To compare the obtained data, the experimental values of the Nèel temperature (T_N, upper line) and spin-flop transition field (H_{SF}, lower line) are plotted as a function of the concentration of A^{IV} = Ge, Pb, Sn in Figure 4. As mentioned previously, the concentration was estimated for the surface of single crystals, which may have slight variations compared to the average element concentration in the bulk. However, for the majority of samples, a relatively sharp AFM peak is observed, suggesting a relatively homogeneous distribution of A^{IV} = Ge, Pb, Sn within the volume. This allows evaluations to be carried out using XPS from surface of a single-crystal. Nevertheless, a sufficiently large error interval of $\pm$0.05 fraction was chosen for the concentration, which is expected to include the actual concentration value. The error in determining the Nèel temperature is $\pm$1 K, and the error in determining the spin-flop transition field is $\pm$0.4 T. The observed changes in the magnetic parameters for samples with adjacent concentrations are generally larger than the associated errors.

Preprints (www.preprints.org) | NOT PEER-REVIEWED | Posted: 25 July 2023 doi:10.20944/preprints202307.1640.v1

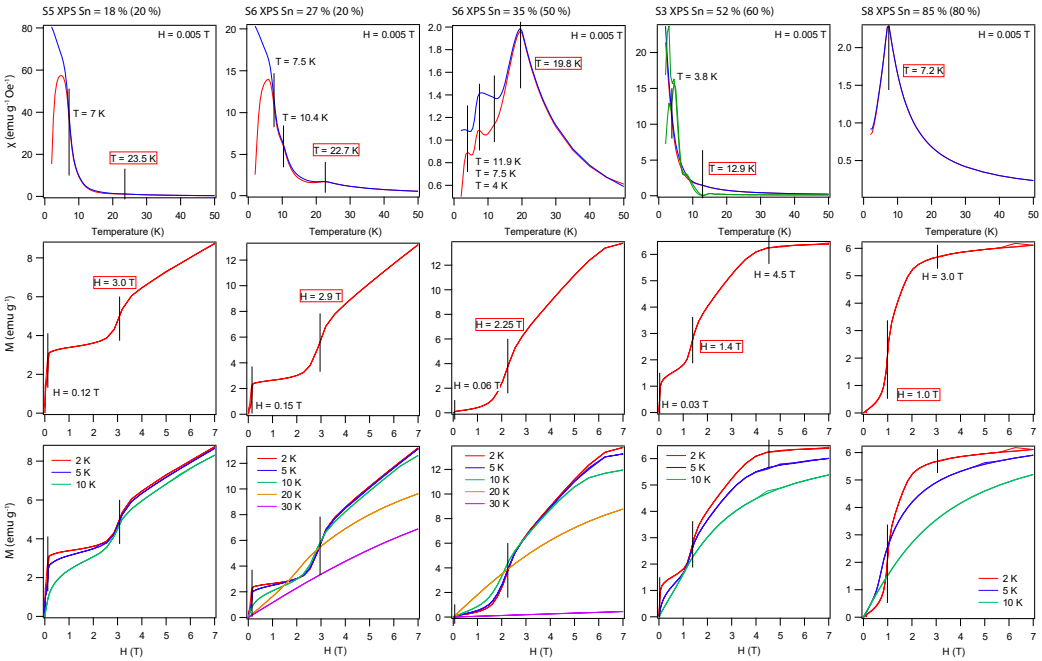

Figure 2. Dependencies of $\chi(T)$ [top line] and M(H) [middle and bottom lines] for $(Mn_{1-x}Sn_x)Bi_2Te_4$ samples. The notation is the same as in Figure 1. The green curve in the $\chi(T)$ panel for Sn = 52 % is $d^2\chi(T)/dT^2$.

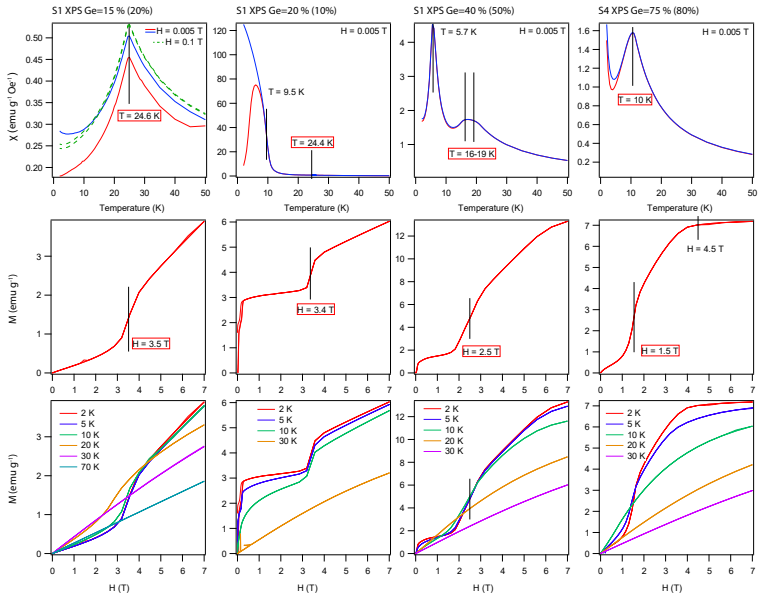

Figure 3. Dependencies of $\chi(T)$ [top line] and M(H) [middle and bottom lines] for $(Mn_{1-x}Ge_x)Bi_2Te_4$ samples. The notation is the same as in Figure 1.

A clear monotonic decrease of T_N and H_{SF} with increasing substitution concentration can be observed for all elements. The experimental data points can be approximated by linear dependencies [30]. The black line represents a linear approximation of the experimental points, while the green line takes into account the expectation that the Nèel temperature and spin-flop transition field reach zero at 100% of A^{IV} = Ge, Pb, Sn.

In the case of $(Mn_{1-x}Pb_x)Bi_2Te_4$, it is evident that the black line reaches zero for both T_N and H_{SF} at Pb concentrations around $80-90\%$. This suggests that Mn-doped $PbBi_2Te_4$ does not exhibit magnetic properties at Mn concentration $(1-x) < 15-20\%$. Thus, it is important to note that a

Preprints (www.preprints.org) | NOT PEER-REVIEWED | Posted: 25 July 2023 doi:10.20944/preprints202307.1640.v1

doping level of approximately 2% (the ratio of impurity in total, which corresponds to a Mn fraction of $(1-x) \approx 15\%$ in the notation used) appears to be sufficient for TIs to demonstrate magnetic properties and transition to the QAHE state, as demonstrated in the case of $Cr_{0.1}(Bi,Sb)_{1.9}Te_3$ [42]. This difference could be attributed to the fact that in magnetically doped TIs, the magnetic impurity replaces Bi atoms in both layers, resulting in close proximity of magnetic atoms. In the case of $(Mn_{1-x}Pb_x)Bi_2Te_4$, however, Mn atoms preferentially replace Pb in the central layer, leading to weaker interaction between Mn atoms across the layers, which prevents the formation of magnetic order.

Regarding $(Mn_{1-x}Sn_x)Bi_2Te_4$ and $(Mn_{1-x}Ge_x)Bi_2Te_4$, the approximation reveals non-zero values of T_N and H_{SF} even at zero Mn concentration. This could indicate either (i) the possibility of nonlinear behavior in the region of high Sn/Ge concentration, resulting in more rapid decrease of T_N and H_{SF} towards zero in that region, or (ii) a potential overestimation of the Sn/Ge concentration in the estimations obtained using XPS from surface of a single-crystal.

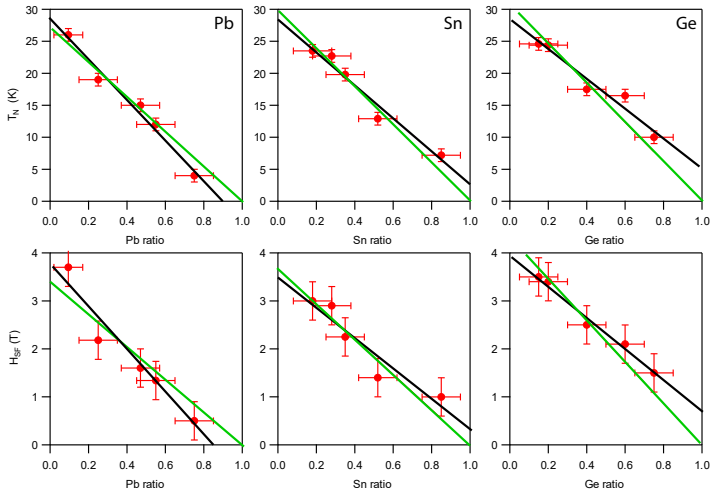

Figure 4. The experimental values of T_N and H_{SF} as a function of the substituent concentration A^{IV} = Ge, Pb, Sn are presented. Linear approximations of the experimental data points (green and black lines) are shown (see details in the text).

From the analysis of the obtained dependencies, it can be observed that the slope of the approximating (black) lines is different for different elements. The steepest slope is observed for $(Mn_{1-x}Pb_x)Bi_2Te_4$, followed by $(Mn_{1-x}Sn_x)Bi_2Te_4$, and the smallest slope is seen for $(Mn_{1-x}Ge_x)Bi_2Te_4$. This indicates that the magnetic parameters change at different rates when Mn is substituted by the corresponding elements. This discrepancy could be attributed to the different rates of increase in the crystal cell size for the different elements. As $PbBi_2Te_4$ has the largest cell size among the three compounds, the change in cell parameters is likely to be most significant for $(Mn_{1-x}Pb_x)Bi_2Te_4$. Hence, the magnetic properties are influenced by the magnetic dilution effect and the changes in cell parameters, as also was analyzed in a previous study [30,43].

Another notable feature is that, based on the linear approximation at zero substitution concentration (i.e., pure $MnBi_2Te_4$), the expected values for T_N and H_{SF} are approximately $27-30$ K and $3.5-4$ T, respectively. These values are higher than the experimentally measured values for pure $MnBi_2Te_4$: T_N = 24.5 K and H_{SF} = 3.5 T. Indeed, for $(Mn_{1-x}Pb_x)Bi_2Te_4$ with a nominal Pb concentration of 10%, the critical parameters exceed those of pure $MnBi_2Te_4$. These results suggest a non-monotonic dependence of the magnetic parameters in the low Pb concentration region. Specifically, adding a small amount of Pb to pure $MnBi_2Te_4$ leads to an increase in T_N and H_{SF}, which then reach a maximum value before starting to decrease.

Hence, the inclusion of a small amount of Pb enhances the magnetic properties of the system. Several explanations can be proposed for this phenomenon. The presence of Pb atoms can decrease the occurrence of Mn_{Bi} anti-site defects. In this case Pb atoms occupy the Bi positions instead of Mn

Preprints (www.preprints.org) | NOT PEER-REVIEWED | Posted: 25 July 2023 doi:10.20944/preprints202307.1640.v1

since Pb_{Bi} anti-site defects may be more energetically favorable due to the similar sizes of Bi and Pb atoms. Consequently, the ferrimagnetic properties of the [$MnBi_2Te_4$] SL can be mitigated. Additionally, the introduction of a small amount of impurity enables structural relaxation, resulting in a more favorable ordering of Mn atoms in the central layer. The obtained results provide evidence supporting such behavior for $(Mn_{1-x}Pb_x)Bi_2Te_4$. In general, similar enhancements in magnetic properties can be expected when Mn is substituted with Sn or Ge.

For the $(Mn_{1-x}Pb_x)Bi_2Te_4$ sample with a nominal concentration of 10%, which exhibited increased magnetic parameters, the temperature-dependent changes in the electronic structure near the Néel temperature region were investigated using ARPES (Figure 5). The analysis of the splitting of Te p_z states can provide insight into the local magnetic properties of the $MnBi_2Te_4$-related system [17]. Figure 5a illustrates the temperature-dependent distribution of states at the Γ-point. Similar to pure $MnBi_2Te_4$, a splitting of the Te p_z states at the edge of the conduction band is observed (indicated by blue dashed lines). The lower part of the panel presents the dependence of the splitting [$\Delta E(T)$] of this state. The experimental data points were fitted with a power law: $\Delta E \sim (1 - T/T_0)^{\beta}$, where β is the critical exponent and T_0 is the onset temperature of the splitting. The obtained values are $T_0 = 26.6$ K and $\beta = 0.38$, which is close to the critical exponent for the 3D Heisenberg case.

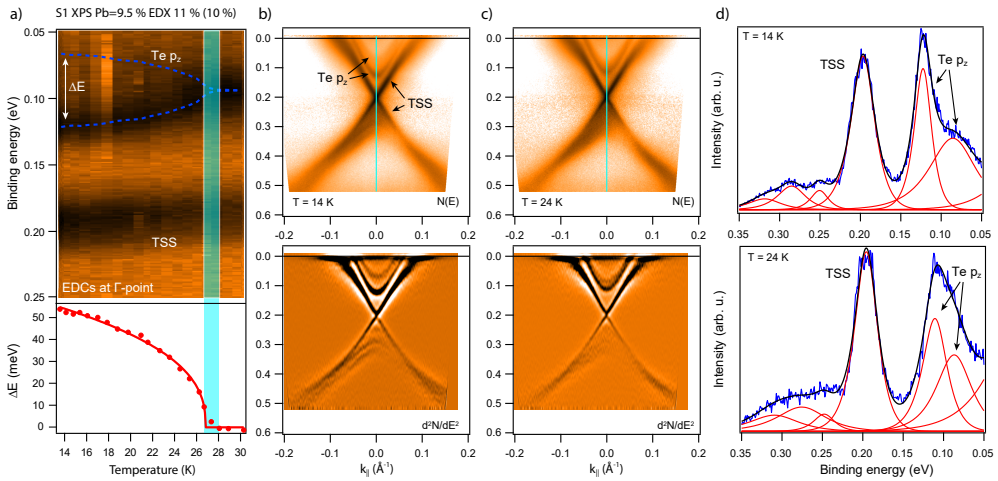

Figure 5. Dispersion relations for $(Mn_{1-x}Pb_x)Bi_2Te_4$ with a nominal Pb concentration of 10%. In panel (a), the temperature dependence of the state distribution at the Γ-point is shown within the range of 14 K to 30 K. The positions of Te p_z states are indicated by blue dashed lines, and the onset of the Te p_z state splitting is marked by a vertical cyan line. The temperature dependence of the Te p_z splitting value is presented at the bottom, as well as its approximation by the power law. Panels (b) and (c) display dispersion relations at 14 K and 24 K, presented as N(E) (top line) and d^2N/dE^2 (bottom line). In panel (d), the decomposition of EDCs at the Γ-point into spectral components are shown. At the top, we provide additional estimates of the Pb content obtained by EDX method directly for the investigated surface. The TSS labels on the panels marks the topological surface states.

In Figure 5b, the dispersion relations measured at 14 K are presented. Panel d (top part) displays the decomposition of the EDC at the Γ-point into spectral components. The splitting of the Te p_z states is clearly observed. Notably, even at T = 24 K (panel c), the states remain split, although the splitting becomes smaller. This can be seen from the EDC decomposition in panel d (bottom part). Overall, the obtained data provide clear evidence for an elevated magnetic ordering temperature of the 124 phase in $(Mn_{1-x}Pb_x)Bi_2Te_4$ at a Pb concentration of approximately 10%.

4. Conclusions

A series of $(Mn_{1-x}A^{IV}_x)Bi_2Te_4$ samples with different levels of Mn substitution by nonmagnetic A^{IV} = Ge, Pb, Sn elements was studied in this work. Overall, similar trends were observed for all

elements: the magnetic ordering temperature and spin-flop transition field decreased with increasing A^{IV} = Ge, Pb, Sn concentration for the 124 phase. The magnetic ordering remained AFM for all substitution levels. However, different rates of change in the magnetic parameters were observed for different elements, with the highest rate for Pb, followed by Sn, and the lowest for Ge. This behavior can be attributed to the combined effects of magnetic dilution and lattice parameter increase, which is most pronounced in the $(Mn_{1-x}Pb_x)Bi_2Te_4$ compound. Furthermore, the linear approximation of the experimental data indicated that pure $MnBi_2Te_4$ could exhibit higher values of the critical parameters than those observed experimentally. This suggests a potential non-monotonic behavior of the magnetic parameters at low substitution concentrations and the possibility of enhancing the magnetic properties through the doping of $MnBi_2Te_4$ with a small amount of nonmagnetic impurity. Indeed, we found $(Mn_{1-x}Pb_x)Bi_2Te_4$ sample with a nominal concentration of 10% that exhibited higher critical parameters compared to $MnBi_2Te_4$, with $T_N \approx 26$ K and $H_{SF} \approx 3.7$ T. The increased Nèel temperature was further confirmed through the analysis of electronic structure changes using the ARPES method.

Author Contributions: Conceptualization, Dmitry Estyunin and Alexander Shikin; Formal analysis, Dmitry Estyunin and Anna Rybkina; Funding acquisition, Alexander Shikin; Investigation, Dmitry Estyunin, Anna Rybkina and Marina Likholetova; Resources, Konstantin Kokh and Oleg Tereshchenko; Validation, Dmitry Estyunin, Anna Rybkina and Alexander Shikin; Visualization, Dmitry Estyunin; Writing – original draft, Dmitry Estyunin; Writing – review and editing, Dmitry Estyunin. All authors have read and agreed to the published version of the manuscript.

Funding: This research was funded by Ministry of Science and Higher Education of the Russian Federation Grant No. 075-15-2020-797 (13.1902.21.0024).

Institutional Review Board Statement: Not applicable.

Informed Consent Statement: Not applicable.

Data Availability Statement: Data will be made available on request.

Acknowledgments: The authors acknowledge the following centers of the Research Park of St. Petersburg University: "Centre for Diagnostics of Functional Materials for Medicine, Pharmacology and Nanoelectronics", where the magnetic properties of the materials were studied, and "Centre for Physical Methods of Surface Investigation" and "Centre for Nanotechnology", where the elemental composition of the samples was studied. The samples studied in this work were synthesised under state assignment of IGM SB RAS 122041400031-2. ARPES measurements were carried out at the HiSOR synchrotron centre under Proposals No. 21AG010; 21AG014; 21BG028; 21BG037. The authors thank N-BARD, Hiroshima University, for supplying liquid He.

Conflicts of Interest: The authors declare no conflict of interest.

Abbreviations

Abbreviations

The following abbreviations are used in this manuscript:

ARPES	Angle-resolved photoemission spectroscopy
AFM, FM, PM	Antiferromagnetic, ferromagnetic, paramagnetic
EDC	Energy distribution curves
EDX	Energy-dispersive X-ray spectroscopy
H_{SF}	Spin-flop transition field
QAHE	Quantum anomalous Hall effect
QL/SL	Quintuple [Bi_2Te_3]/ septuple [$MnBi_2Te_4$] layers block
SQUID	Superconducting quantum interference device
TI	Topological insulator
T_N	Nèel temperature
XPS	X-ray photoemission spectroscopy
ZFC, FC	Zero field cooled, field cooled
Phases 124, 147, $16\overline{10}$	$(Mn_{1-x}A^{IV}_x)Bi_{2m}Te_{3m+1}$ with m = 1,2,3 (A^{IV} = Ge, Pb, Sn)

References

1. Chang, C.Z.; Li, M. Quantum anomalous Hall effect in time-reversal-symmetry breaking topological insulators. *Journal of Physics: Condensed Matter* **2016**, *28*, 123002.
2. He, K.; Xue, Q.K. The Road to High-Temperature Quantum Anomalous Hall Effect in Magnetic Topological Insulators. *SPIN* **2019**, *09*, 1940016. doi:10.1142/s2010324719400162.
3. Giustino, F.; Lee, J.H.; Trier, F.; Bibes, M.; Winter, S.M.; Valentí, R.; Son, Y.W.; Taillefer, L.; Heil, C.; Figueroa, A.I.; Plaçais, B.; Wu, Q.; Yazyev, O.V.; Bakkers, E.P.A.M.; Nygård, J.; Forn-Díaz, P.; De Franceschi, S.; McIver, J.W.; Torres, L.E.F.F.; Low, T.; Kumar, A.; Galceran, R.; Valenzuela, S.O.; Costache, M.V.; Manchon, A.; Kim, E.A.; Schleder, G.R.; Fazzio, A.; Roche, S. The 2021 quantum materials roadmap. *Journal of Physics: Materials* **2021**, *3*, 042006.
4. Chang, C.Z.; Liu, C.X.; MacDonald, A.H. Colloquium: Quantum anomalous Hall effect. *Rev. Mod. Phys.* **2023**, *95*, 011002. doi:10.1103/RevModPhys.95.011002.
5. Otrokov, M.M.; Rusinov, I.P.; Blanco-Rey, M.; Hoffmann, M.; Vyazovskaya, A.Y.; Eremeev, S.V.; Ernst, A.; Echenique, P.M.; Arnau, A.; Chulkov, E.V. Unique Thickness-Dependent Properties of the van der Waals Interlayer Antiferromagnet $MnBi_2Te_4$ Films. *Phys. Rev. Lett.* **2019**, *122*, 107202. doi:10.1103/PhysRevLett.122.107202.
6. Otrokov, M.M.; Klimovskikh, I.I.; Bentmann, H.; Estyunin, D.; Zeugner, A.; Aliev, Z.S.; Gaß, S.; Wolter, A.U.B.; Koroleva, A.V.; Shikin, A.M.; Blanco-Rey, M.; Hoffmann, M.; Rusinov, I.P.; Vyazovskaya, A.Y.; Eremeev, S.V.; Koroteev, Y.M.; Kuznetsov, V.M.; Freyse, F.; Sánchez-Barriga, J.; Amiraslanov, I.R.; Babanly, M.B.; Mamedov, N.T.; Abdullayev, N.A.; Zverev, V.N.; Alfonsov, A.; Kataev, V.; Büchner, B.; Schwier, E.F.; Kumar, S.; Kimura, A.; Petaccia, L.; Di Santo, G.; Vidal, R.C.; Schatz, S.; Kißner, K.; Ünzelmann, M.; Min, C.H.; Moser, S.; Peixoto, T.R.F.; Reinert, F.; Ernst, A.; Echenique, P.M.; Isaeva, A.; Chulkov, E.V. Prediction and observation of an antiferromagnetic topological insulator. *Nature* **2019**, *576*, 416–422.
7. Zhang, D.; Shi, M.; Zhu, T.; Xing, D.; Zhang, H.; Wang, J. Topological Axion States in the Magnetic Insulator $MnBi_2Te_4$ with the Quantized Magnetoelectric Effect. *Phys. Rev. Lett.* **2019**, *122*, 206401. doi:10.1103/PhysRevLett.122.206401.
8. Li, J.; Li, Y.; Du, S.; Wang, Z.; Gu, B.L.; Zhang, S.C.; He, K.; Duan, W.; Xu, Y. Intrinsic magnetic topological insulators in van der Waals layered $MnBi_2Te_4$-family materials. *Sci Adv* **2019**, *5*, eaaw5685.
9. Gong, Y.; Guo, J.; Li, J.; Zhu, K.; Liao, M.; Liu, X.; Zhang, Q.; Gu, L.; Tang, L.; Feng, X.; Zhang, D.; Li, W.; Song, C.; Wang, L.; Yu, P.; Chen, X.; Wang, Y.; Yao, H.; Duan, W.; Xu, Y.; Zhang, S.C.; Ma, X.; Xue, Q.K.; He, K. Experimental Realization of an Intrinsic Magnetic Topological Insulator. *Chinese Physics Letters* **2019**, *36*, 076801.
10. Deng, Y.; Yu, Y.; Shi, M.Z.; Guo, Z.; Xu, Z.; Wang, J.; Chen, X.H.; Zhang, Y. Quantum anomalous Hall effect in intrinsic magnetic topological insulator $MnBi_2Te_4$. *Science* **2020**, *367*, 895.
11. Liu, C.; Wang, Y.; Li, H.; Wu, Y.; Li, Y.; Li, J.; He, K.; Xu, Y.; Zhang, J.; Wang, Y. Robust axion insulator and Chern insulator phases in a two-dimensional antiferromagnetic topological insulator. *Nature Materials* **2020**, *19*, 522–527.
12. Ge, J.; Liu, Y.; Li, J.; Li, H.; Luo, T.; Wu, Y.; Xu, Y.; Wang, J. High-Chern-number and high-temperature quantum Hall effect without Landau levels. *National Science Review* **2020**, *7*, 1280–1287.
13. Lee, D.S.; Kim, T.H.; Park, C.H.; Chung, C.Y.; Lim, Y.S.; Seo, W.S.; Park, H.H. Crystal structure, properties and nanostructuring of a new layered chalcogenide semiconductor, Bi2MnTe4. *CrystEngComm* **2013**, *15*, 5532–5538.
14. Aliev, Z.S.; Amiraslanov, I.R.; Nasonova, D.I.; Shevelkov, A.V.; Abdullayev, N.A.; Jahangirli, Z.A.; Orujlu, E.N.; Otrokov, M.M.; Mamedov, N.T.; Babanly, M.B.; Chulkov, E.V. Novel ternary layered manganese bismuth tellurides of the MnTe-Bi2Te3 system: Synthesis and crystal structure. *Journal of Alloys and Compounds* **2019**, *789*, 443–450.
15. Yan, J.Q.; Zhang, Q.; Heitmann, T.; Huang, Z.; Chen, K.Y.; Cheng, J.G.; Wu, W.; Vaknin, D.; Sales, B.C.; McQueeney, R.J. Crystal growth and magnetic structure of $MnBi_2Te_4$. *Phys. Rev. Materials* **2019**, *3*, 064202. doi:10.1103/PhysRevMaterials.3.064202.
16. Li, H.; Liu, S.; Liu, C.; Zhang, J.; Xu, Y.; Yu, R.; Wu, Y.; Zhang, Y.; Fan, S. Antiferromagnetic topological insulator MnBi2Te4: synthesis and magnetic properties. *Phys. Chem. Chem. Phys.* **2020**, *22*, 556–563.

17. Estyunin, D.A.; Klimovskikh, I.I.; Shikin, A.M.; Schwier, E.F.; Otrokov, M.M.; Kimura, A.; Kumar, S.; Filnov, S.O.; Aliev, Z.S.; Babanly, M.B.; Chulkov, E.V. Signatures of temperature driven antiferromagnetic transition in the electronic structure of topological insulator $MnBi_2Te_4$. *APL Materials* **2020**, *8*, 021105. doi:10.1063/1.5142846.
18. Lai, Y.; Ke, L.; Yan, J.; McDonald, R.D.; McQueeney, R.J. Defect-driven ferrimagnetism and hidden magnetization in $MnBi_2Te_4$. *Phys. Rev. B* **2021**, *103*, 184429. doi:10.1103/PhysRevB.103.184429.
19. Wu, J.; Liu, F.; Sasase, M.; Ienaga, K.; Obata, Y.; Yukawa, R.; Horiba, K.; Kumigashira, H.; Okuma, S.; Inoshita, T.; Hosono, H. Natural van der Waals heterostructural single crystals with both magnetic and topological properties. *Science Advances* **2019**, *5*, eaax9989. doi:10.1126/sciadv.aax9989.
20. Hu, C.; Gordon, K.N.; Liu, P.; Liu, J.; Zhou, X.; Hao, P.; Narayan, D.; Emmanouilidou, E.; Sun, H.; Liu, Y.; Brawer, H.; Ramirez, A.P.; Ding, L.; Cao, H.; Liu, Q.; Dessau, D.; Ni, N. A van der Waals antiferromagnetic topological insulator with weak interlayer magnetic coupling. *Nature Communications* **2020**, *11*, 97.
21. Klimovskikh, I.I.; Otrokov, M.M.; Estyunin, D.; Eremeev, S.V.; Filnov, S.O.; Koroleva, A.; Shevchenko, E.; Voroshnin, V.; Rybkin, A.G.; Rusinov, I.P.; Blanco-Rey, M.; Hoffmann, M.; Aliev, Z.S.; Babanly, M.B.; Amiraslanov, I.R.; Abdullayev, N.A.; Zverev, V.N.; Kimura, A.; Tereshchenko, O.E.; Kokh, K.A.; Petaccia, L.; Di Santo, G.; Ernst, A.; Echenique, P.M.; Mamedov, N.T.; Shikin, A.M.; Chulkov, E.V. Tunable 3D/2D magnetism in the $(MnBi_2Te_4)(Bi_2Te_3)_m$ topological insulators family. *npj Quantum Materials* **2020**, *5*, 54.
22. Shikin, A.M.; Estyunin, D.A.; Glazkova, D.A.; Fil'nov, S.O.; Klimovskikh, I.I. Electronic and Spin Structures of Intrinsic Antiferromagnetic Topological Insulators of the $MnBi_2Te_4(Bi_2Te_3)_m$ Family and Their Magnetic Properties (Brief Review). *JETP Letters* **2022**, *115*, 213–225.
23. Yan, C.; Zhu, Y.; Miao, L.; Fernandez-Mulligan, S.; Green, E.; Mei, R.; Tan, H.; Yan, B.; Liu, C.X.; Alem, N.; Mao, Z.; Yang, S. Delicate Ferromagnetism in $MnBi_6Te_{10}$. *Nano Lett.* **2022**, *22*, 9815–9822. doi:10.1021/acs.nanolett.2c02500.
24. Tcakaev, A.V.; Rubrecht, B.; Facio, J.I.; Zabolotnyy, V.B.; Corredor, L.T.; Folkers, L.C.; Kochetkova, E.; Peixoto, T.R.F.; Kagerer, P.; Heinze, S.; Bentmann, H.; Green, R.J.; Gargiani, P.; Valvidares, M.; Weschke, E.; Haverkort, M.W.; Reinert, F.; van den Brink, J.; Büchner, B.; Wolter, A.U.B.; Isaeva, A.; Hinkov, V. Intermixing-Driven Surface and Bulk Ferromagnetism in the Quantum Anomalous Hall Candidate $MnBi_6Te_{10}$. *Adv. Sci.* **2023**, *10*, 2203239.
25. Chen, B.; Fei, F.; Zhang, D.; Zhang, B.; Liu, W.; Zhang, S.; Wang, P.; Wei, B.; Zhang, Y.; Zuo, Z.; Guo, J.; Liu, Q.; Wang, Z.; Wu, X.; Zong, J.; Xie, X.; Chen, W.; Sun, Z.; Wang, S.; Zhang, Y.; Zhang, M.; Wang, X.; Song, F.; Zhang, H.; Shen, D.; Wang, B. Intrinsic magnetic topological insulator phases in the Sb doped MnBi2Te4 bulks and thin flakes. *Nature Communications* **2019**, *10*, 4469.
26. Murakami, T.; Nambu, Y.; Koretsune, T.; Xiangyu, G.; Yamamoto, T.; Brown, C.M.; Kageyama, H. Realization of interlayer ferromagnetic interaction in $MnSb_2Te_4$ toward the magnetic Weyl semimetal state. *Phys. Rev. B* **2019**, *100*, 195103. doi:10.1103/PhysRevB.100.195103.
27. Liu, Y.; Wang, L.L.; Zheng, Q.; Huang, Z.; Wang, X.; Chi, M.; Wu, Y.; Chakoumakos, B.C.; McGuire, M.A.; Sales, B.C.; Wu, W.; Yan, J. Site Mixing for Engineering Magnetic Topological Insulators. *Phys. Rev. X* **2021**, *11*, 021033. doi:10.1103/PhysRevX.11.021033.
28. Kuznetsova, L.A.; Kuznetsov, V.L.; Rowe, D.M. Thermoelectric properties and crystal structure of ternary compounds in the Ge(Sn,Pb)Te-Bi_2Te_3 systems. *Journal of Physics and Chemistry of Solids* **2000**, *61*, 1269–1274.
29. Zhu, J.; Naveed, M.; Chen, B.; Du, Y.; Guo, J.; Xie, H.; Fei, F. Magnetic and electrical transport study of the antiferromagnetic topological insulator Sn-doped $MnBi_2Te_4$. *Phys. Rev. B* **2021**, *103*, 144407. doi:10.1103/PhysRevB.103.144407.
30. Qian, T.; Yao, Y.T.; Hu, C.; Feng, E.; Cao, H.; Mazin, I.I.; Chang, T.R.; Ni, N. Magnetic dilution effect and topological phase transitions in $(Mn_{1-x}Pb_x)Bi_2Te_4$. *Phys. Rev. B* **2022**, *106*, 045121. doi:10.1103/PhysRevB.106.045121.
31. Changdar, S.; Ghosh, S.; Vijay, K.; Kar, I.; Routh, S.; Maheshwari, P.K.; Ghorai, S.; Banik, S.; Thirupathaiah, S. Nonmagnetic Sn doping effect on the electronic and magnetic properties of antiferromagnetic topological insulator $MnBi_2Te_4$. *Physica B: Condensed Matter* **2023**, *657*, 414799.
32. Frolov, A.S.; Usachov, D.Y.; Tarasov, A.V.; Fedorov, A.V.; Bokai, K.A.; Klimovskikh, I.; Stolyarov, V.S.; Sergeev, A.I.; Lavrov, A.N.; Golyashov, V.A.; Tereshchenko, O.E.; Santo, G.D.; Petaccia, L.; Clark, O.J.; Sanchez-Barriga, J.; Yashina, L.V. Magnetic Dirac semimetal state of (Mn,Ge)Bi_2Te_4, 2023, [arXiv:cond-mat.mtrl-sci/2306.13024].

33. Tarasov, A.V.; Makarova, T.P.; Estyunin, D.A.; Eryzhenkov, A.V.; Klimovskikh, I.I.; Golyashov, V.A.; Kokh, K.A.; Tereshchenko, O.E.; Shikin, A.M. Topological Phase Transitions Driven by Sn Doping in $(Mn_{1-x}Sn_x)Bi_2Te_4$. *Symmetry* **2023**, *15*. doi:10.3390/sym15020469.
34. Chen, W.Q.; Teo, K.L.; Jalil, M.B.A.; Liew, T. Compositional dependencies of ferromagnetic $Ge_{1-x}Mn_xTe$ grown by solid-source molecular-beam epitaxy. *Journal of Applied Physics* **2006**, *99*, 08D515.
35. Hassan, M.; Springholz, G.; Lechner, R.T.; Groiss, H.; Kirchschlager, R.; Bauer, G. Molecular beam epitaxy of single phase GeMnTe with high ferromagnetic transition temperature. *Journal of Crystal Growth* **2011**, *323*, 363–367.
36. Ren, Z.; Taskin, A.A.; Sasaki, S.; Segawa, K.; Ando, Y. Optimizing $\mathbf{Bi}_{2-x}\mathbf{Sb}_x\mathbf{Te}_{3-y}\mathbf{Se}_y$ solid solutions to approach the intrinsic topological insulator regime. *Phys. Rev. B* **2011**, *84*, 165311. doi:10.1103/PhysRevB.84.165311.
37. Xu, Y.; Miotkowski, I.; Liu, C.; Tian, J.; Nam, H.; Alidoust, N.; Hu, J.; Shih, C.K.; Hasan, M.Z.; Chen, Y.P. Observation of topological surface state quantum Hall effect in an intrinsic three-dimensional topological insulator. *Nature Physics* **2014**, *10*, 956–963.
38. Kokh, K.A.; Makarenko, S.V.; Golyashov, V.A.; Shegai, O.A.; Tereshchenko, O.E. Melt growth of bulk Bi2Te3 crystals with a natural p-n junction. *CrystEngComm* **2014**, *16*, 581–584.
39. Kokh, K.A.; Andreev, Y.M.; Svetlichnyi, V.A.; Lanskii, G.V.; Kokh, A.E. Growth of GaSe and GaS single crystals. *Cryst. Res. Technol.* **2011**, *46*, 327–330.
40. Iwasawa, H.; Schwier, E.F.; Arita, M.; Ino, A.; Namatame, H.; Taniguchi, M.; Aiura, Y.; Shimada, K. Development of laser-based scanning μ-ARPES system with ultimate energy and momentum resolutions. *Ultramicroscopy* **2017**, *182*, 85–91.
41. Szuszkiewicz, W.; Hennion, B.; Witkowska, B.; Łusakowska, E.; Mycielski, A. Neutron scattering study of structural and magnetic properties of hexagonal MnTe. *physica status solidi (c)* **2005**, *2*, 1141–1146. doi:10.1002/pssc.200460669.
42. Mogi, M.; Yoshimi, R.; Tsukazaki, A.; Yasuda, K.; Kozuka, Y.; Takahashi, K.S.; Kawasaki, M.; Tokura, Y. Magnetic modulation doping in topological insulators toward higher-temperature quantum anomalous Hall effect. *Appl. Phys. Lett.* **2015**, *107*, 182401. doi:10.1063/1.4935075.
43. Chen, K.Y.; Wang, B.S.; Yan, J.Q.; Parker, D.S.; Zhou, J.S.; Uwatoko, Y.; Cheng, J.G. Suppression of the antiferromagnetic metallic state in the pressurized $MnBi_2Te_4$ single crystal. *Phys. Rev. Mater.* **2019**, *3*, 094201. doi:10.1103/PhysRevMaterials.3.094201.